reviewed paper VisionEducation

Integrating Urban Master Plan Scenarios with Climate Projections to Model Future Urban Heat Island Dynamics in Erbil, Iraq

Mohammed Mirza Agha Mahmood, Hushiar Raheem Hamarash

(Mohammed Mirza Agha Mahmood, Soran University, Scientific Research Center, Soran, Iraq; mohammed.mahmood@soran.edu.iq)
(Hushiar Raheem Hamarash, Soran University, Scientific Research Center, Soran, Iraq; hrh670h@src.soran.edu.iq)

DOI: 10.48494/REALCORP2026.5099

1 ABSTRACT

The current study focuses on the trends of LST in Erbil city in Iraq under urban development and climate change using remote sensing analysis. Landsat 5 TM, Landsat 8 OLI/TIRS, and Landsat 9 data were obtained in 2009, 2014, 2019, and 2024 and processed using ArcGIS Pro, Google Earth Engine, and ERDAS Imagine. The land use/land cover (LU/LC) maps were created based on the supervised classification using the Maximum Likelihood classifier, with overall accuracy ranging from 91.4% to 94.7%. Results showed that built-up area increased from 19.42% in 2009 to 29.04% in 2024, and barren land decreased from 79.40% to 66.91%. Furthermore, the highest maximum LST increased from 51°C in 2009 to 54.3°C in 2024, whereas UHI intensity was found to be 22.5°C in 2019. According to the SSP2-4.5 and SSP5-8.5 scenarios, LST is forecasted to become 55.0°C and 56.7°C in 2050, respectively. A mitigation scenario with the implementation of Erbil Green Belt master plan (165.35 km² with 7.2 million olive and pistachio trees) was investigated, leading to an increment in the NDVI to 0.5 and a decrease in the temperature to -2.5°C and -0.4°C in the Green Belt and urban zones, respectively.

Keywords: urban development, climate change, built-up area, green belt, Erbil

2 INTRODUCTION

In addition, rapid urbanization and changes in the climate are altering the thermal conditions of cities worldwide. The world population is expected to increase to 9.7 billion people by 2050. The population living in cities is also expected to increase, thus increasing the pressure for land use and infrastructure expansion. (United Nations, 2019). Generally, urban expansion tends to change the original surfaces from natural or agricultural types to impervious surfaces such as concrete, asphalt, and roofs, which changes the energy balance of the surfaces and increases the amount of heat exposure, particularly in areas of urban expansion. (Seto et al., 2012; IPCC, 2021).

One of the major indicators of these changes is the Urban Heat Island (UHI) effect, where the urban area tends to be hotter than the rural area due to the reduction of evapotranspiration and increase in the storage of heat. (Oke, 1982; Voogt and Oke, 2003). For instance, in semi-arid conditions, the thermal contrasts may be large, especially considering that dry soils and surfaces with little vegetation are prone to rapid heating with the intense solar irradiance, while irrigated green spaces provide unique microclimates for cooling. (Zhou et al., 2014; Rasul, Balzter and Smith, 2016). The arrangement and form of the city also play an important role, especially considering the density and verticality of buildings, which enhance the trapping of radiative heat. (Santamouris, 2015). Land Surface Temperature (LST), as a key parameter, is essential in assessing urban thermal environments, as it represents the spatial distribution of surface heating of different land cover classes (Weng, 2009). Multi-temporal studies have confirmed that LST is primarily driven by the composition of land use/land cover (LU/LC), with built-up areas and barren classes being warmer, and vegetation being cooler due to shading and evapotranspiration effects (Weng, Lu and Schubring, 2004; El-Zeiny and Effat, 2017). Vegetation metrics, like the Normalized Difference Vegetation Index (NDVI), are frequently used to study urban cooling effects, and several studies have found a negative relationship between NDVI and land surface temperature (LST) in summer season. (Pettorelli et al., 2005; Weng, 2009).

Erbil city, located in the Kurdistan Region of Iraq, is characterized as a semi-arid urban center with remarkable urbanization dynamics and considerable changes in its land use and land cover (LU/LC) characteristics, especially during the last two decades of the 21st century, with changes in thermal dynamics as reported by previous studies based on remote sensing approaches. (Rasul, Balzter and Smith, 2017). The present study contributes to the aim of establishing the link between the thermal dynamics of the past and the modeling of future thermal scenario projections by integrating LU/LC, NDVI, LST, and UHI analysis of the

period 2009-2024 and the climate change scenario projections of 2050 under SSP2-4.5 and SSP5-8.5, and the mitigation scenario of the Green Belt of the Urban Master Plan. Specifically, the objectives of the present study are: (1) to determine the LU/LC changes, (2) to analyze the LST and UHI changes, (3) to examine the NDVI-LST relationship, and (4) to evaluate the 2050 LST and UHI thermal scenario projections under the two climate change projections and the mitigation scenario of the Green Belt of the Urban. This research addresses this knowledge gap by integrating multi-temporal Landsat-based land use/land cover, normalized difference vegetation index, LST, and UHI studies (2009-2024) with SSP-based climate projections in 2050, as well as a planning-oriented greening scenario.

3 MATERIALS AND METHODS

3.1 Study Area

Erbil is one of the major cities in the Kurdistan Region of Iraq. It is also the capital of this region. The city is located between Duhok Province to its west and Sulaymaniyah Province to its east. It is located at approximately 36°08'N to 36°14'N in latitude and 43°57'E to 44°03'E in longitude (figure1). The city is located at an elevated position of 426 meters above sea level, and its total area is 14,873.68 km2, whereas the study area covers an area of 646.25 km2. In the last two decades, the city has recorded remarkable growth, and its population reached 1,530,722 people by 2015, indicating a growth rate of 2.9%. (Kovács, F., & Tobak, Z. 2017. Hussein,Kovács and Tobak, 2017). It has semi-arid and continental climatic features. When examined using the Köppen climate classification system, it falls under a semi-arid and semi-warm climate type (BSh). The mean annual temperature is 21.85°C, with a maximum of 49°C during summer. (Rasul, Balzter and Smith, 2015).

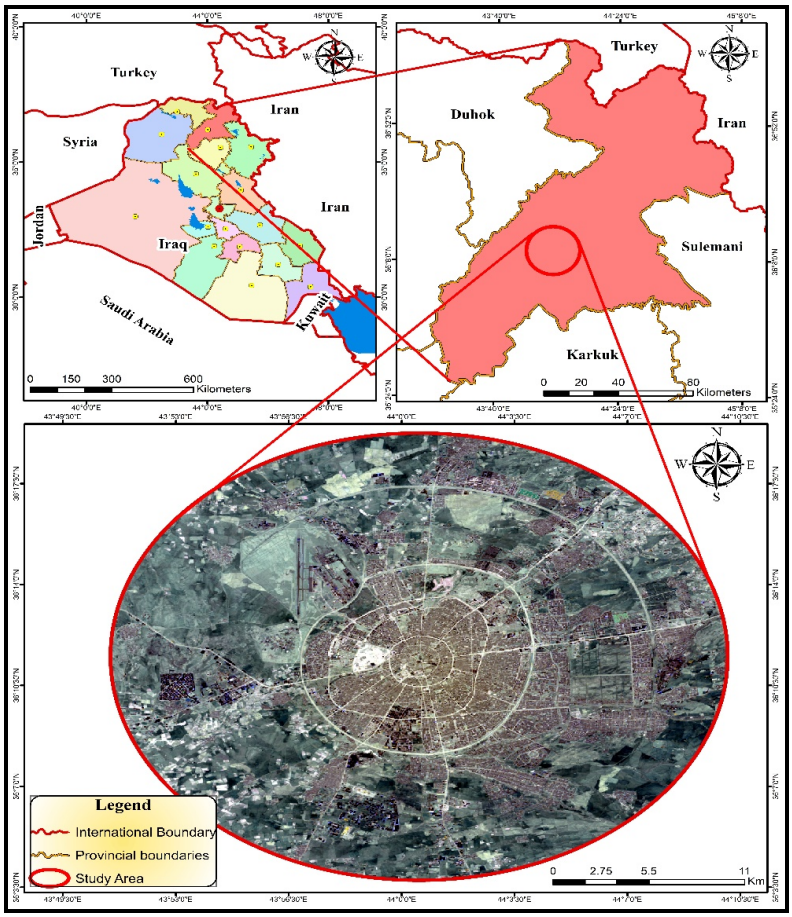

Figure 1: location of the study area. Erbil City

3.2 Used Data

For the purpose of this study, the data used for the integration of the urban master plan scenarios and the climate projections for the modelling of the Land Surface Temperature (LST) is categorized into the following three categories.

The first category of the data is the satellite images provided by the United States Geological Survey (USGS). In this study, the satellite images provided by the USGS using the Landsat 5 TM, Landsat 8 OLI/TIRS, and Landsat 9 images for the years 2009, 2014, 2019, and 2024 were used. These images were taken during the summer season (July-August). The optical bands have a spatial resolution of 30 meters, whereas the thermal bands have a spatial resolution of 100-120 meters and were resampled to 30 meters (Table 1).

The second category of the data is the climate data, which includes the ERA5 2-meter air temperature summer means for the background climatic data.

The third category of the data is the vector data, which includes the Erbil Master Plan 2024, the administrative boundaries, and the land use/land cover maps.

Landsat 4-5 Thematic Mapper (TM) Satellite Image			
Band Number	Wavelength	Resolution	Band Name
Band 1	0.45-0.52	30	Blue
Band 2	0.52-0.60	30	Green
Band 3	0.63-0.69	30	Red
Band 4	0.77-0.90	30	Near IR
Band 5	1.55-1.75	30	Mid IR
Band 6	10.40-12.50	120 (30)	Thermal
Band 7	2.09-2.35	30	Mid IR
Details Of Landsat 8-OLI Satellite Images			
Band Number	Wavelength	Resolution	Band Name
Band 1	0.43-0.45	30	Coastal aerosol
Band 2	0.45-0.51	30	Blue
Band 3	0.53-0.59	30	Green
Band 4	0.64-0.67	30	Red
Band 5	0.85-0.88	30	Near Infrared (NIR)
Band 6	1.57-1.65	30	SWIR 1
Band 7	2.11-2.29	30	SWIR 2
Band 8	0.50-0.68	15	Panchromatic
Band 9	1.36-1.38	30	Cirrus
Band 10	10.6-11.19	100	Thermal Infrared (TIRS) 1
Band 11	11.50-12.51	100	Thermal Infrared (TIRS) 2

Table 1: Spectral Characteristics of Landsat 4-5 Thematic Mapper (TM) Sensor and Landsat 8-9 OLI/TIRS Sensor. Source: https://www.usgs.gov/landsat-missions

3.3 Methodology

This research used ArcGIS Pro software, Google Earth Engine and ERDAS Imagine to investigate spatiotemporal variations of land use/land cover change, NDVI, surface temperature, and urban island intensity in Erbil city (Figure 2). Landsat Level 2 imagery data from Landsat 5 TM, Landsat 8 OLI/TIRS, and Landsat 9 OLI/TIRS were provided by US Geological Survey for 2009, 2014, 2019, and 2024. For each year, three images of summer season (July-August) with cloud cover below 10% were selected. Images were geometrically and atmospherically corrected as Level 2 products. Annual images of land use/land cover change, NDVI, surface temperature, and urban island intensity were created by combining all images of each year to reduce noise and increase representativeness of images acquired during summer season.

Optical bands were used for supervised land use/land cover classification and accuracy assessment. Confusion matrix metrics were used for accuracy assessment. These metrics include overall accuracy, producer's accuracy, user's accuracy, and Kappa. Normalized Difference Vegetation Index (NDVI) was calculated using red and near-infrared bands for each year. Thermal bands were used for calculating land surface temperature (LST) through various conversion steps: conversion of digital number values to radiance values and then to brightness temperature with emissivity correction. Urban heat island (UHI) intensity was calculated using urban-reference temperature difference methods. LST and NDVI were used for baseline

analysis through linear regression for quantifying vegetation-temperature relationship. For future analysis, ERA5-Land summer 2-meter air temperature was modified using an additive delta method with IPCC AR6 projection data (seasonal summer mean deltas). SSP2-4.5 and SSP5-8.5 were used for generating LST scenario maps for 2050 (Figure 2).

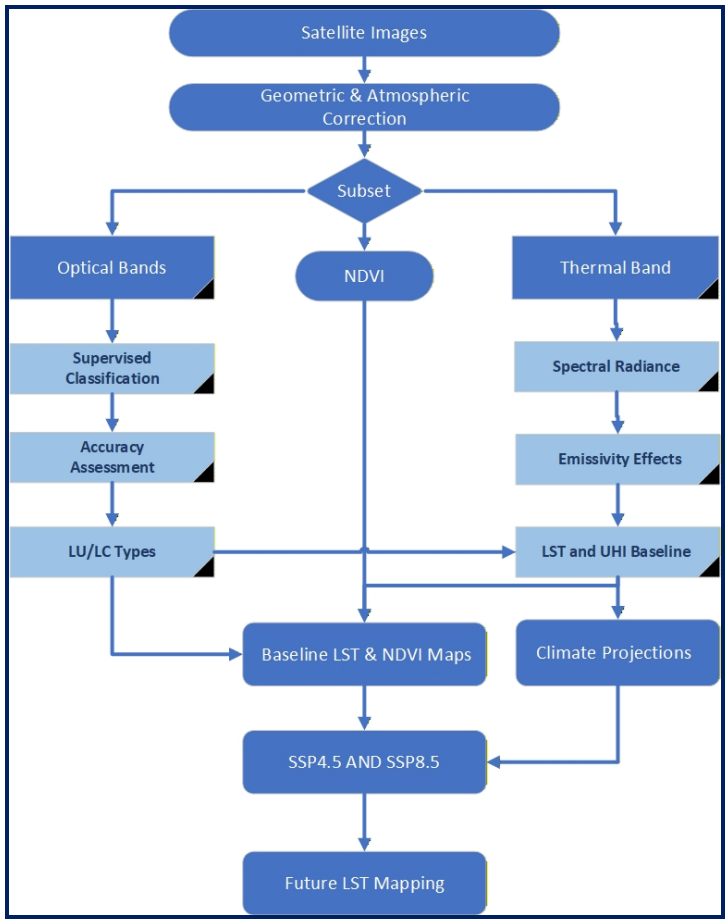

Figure 2: Flow Chart Showing Used Methodology

3.3.1 Image Classification and Accuracy Assessment

Multi-temporal Landsat imagery was used to generate land use/land cover (LU/LC) maps for 2009, 2014, 2019, and 2024. The classification was used to extract three major land use/land cover classes of interest in the region: built-up land, vegetation land, and barren land (Table 2). (Weng, 2009).

For training samples of each class, a selection was done manually by interpreting the satellite images visually and using the knowledge of the study area. At least 40 training pixels per class were collected to account for the spectral variations. The Maximum Likelihood Classification (MLC) algorithm was used to perform the classification of the images (Jensen, 2015). In order to validate the classification results, an accuracy assessment has been carried out using a validation set of data collected through field observation and the interpretation of satellite images. In this regard, a confusion matrix has been used to obtain Overall Accuracy (OA), Producer's Accuracy (PA), User's Accuracy (UA), and the Kappa coefficient (κ). (Congalton and Green, 2019). The classification results were considered reliable if the accuracy level was greater than 85%, and the Kappa statistics indicated substantial agreement. The generated land use/land cover maps were used as the baseline input to simulate the urban heat patterns and assess the possible urban master plan and climate projection scenarios.

Types of LU/LC	Description
BUILT-UP LAND	Residential, industrial, commercial areas, areas under construction, roads and streets
VEGETATION LAND	Types of vegetation include urban green spaces and parks and agricultural lands
BARREN LAND	Sparsely vegetated, including those that have never been used before.

Table 2 : Types of land use and land cover.

3.3.2 Normalized Difference Vegetation Index (NDVI)

Normalized Difference Vegetation Index (NDVI) is a widely used spectral index for assessing the condition and density of vegetation. It makes it easy to differentiate between vegetated and non-vegetated areas using the spectral response of vegetation in the red and near-infrared (NIR) regions.

NDVI was calculated using the standard equation: $NDVI = \frac{(NIR-Red)}{(NIR+Red)}$

Here, NIR represents the near infrared band, whereas Red represents the red band. In the case of the Landsat TM satellite, (Yue et al., 2007; Julien and Sobrino, 2009; Karnieli et al., 2010).

3.3.3 Computation of Land Surface Temperature (LST)

The Land Surface Temperature (LST) estimation used the mono-window algorithm. The mono-window algorithm is a widely used approach for estimating LST from a single band of thermal infrared imagery. (Qin, Karnieli and Berliner, 2001; Rongali, Keshari and Gosain, 2018). The Thermal Band 6 of Landsat TM and Thermal Band 10 of Landsat 8 OLI/TIRS were used. First of all, digital numbers (DN) were converted to spectral radiance by: $L(\lambda) = \text{gain} \times DN + \text{offset}$

Or $L(\lambda) = \frac{L_{max}-L_{min}}{255} \times DN + L_{min}$

Where:

L(λ) = Spectral radiance ($W \cdot sr^{-1} \cdot m^{-2} \cdot \mu m^{-1}$)

LMIN = 1.238 (Spectral radiance of DN value 1)

LMAX = 15.600 (Spectral radiance of DN value 255)

DN = Digital Number

Second, spectral radiance was converted to brightness temperature (TB) in Kelvin using:

$$T_B = \frac{K_2}{\ln\left(\frac{K_1}{L(\lambda)}+1\right)}$$

Where:

K1 = Calibration Constant 1 (607.76)

K2 = Calibration Constant 2 (1260.56)

R = Radiance value ($W/m^2 \cdot sr \cdot \mu m$)

ln = Natural logarithm

Finally, brightness temperature was converted to Celsius: $LST(^\circ C) = T_B(K) - 273.15$

3.3.4 Urban Heat Island (UHI) Analysis

Generally, the intensity of Urban Heat Island (UHI) has been defined as the differential temperature between the urban areas and their reference non-urban environments, usually computed using satellite-derived land surface temperature (LST) data. (Weng, 2009; Zhou et al., 2014). In the present study, the intensity of the UHI has been computed by comparing the average temperature of the built-up areas and the average temperature of the non-urban areas.

$$UHI = T_{urban} - T_{ref}$$

where T_{urban} is the mean temperature of built-up areas and T_{ref} is the mean temperature of vegetation or open land areas.

For spatial analysis, pixel-based UHI intensity was computed as:

$$UHI_{pixel} = T_{pixel} - T_{ref}$$

The positive values of UHI were used to assess the impact of urban expansion.

The ERA5 product represents the fifth generation of ECMWF's atmospheric reanalysis data and offers hourly climate variables on a global scale with high spatial and temporal consistency (Hersbach et al., 2020). ERA5-Land offers improved surface resolution and is frequently used to analyze regional climate. (Muñoz-Sabater et al., 2021).

In this research study, ERA5-Land hourly data were used to obtain the 2-meter air temperature for the study area during the summer season (July and August) for the years 2009, 2014, 2019, and 2024. The average temperature during the summer season was calculated for each study year to determine a climatic baseline for modeling.

To obtain future projections, the ERA5 baseline climate data were modified according to the IPCC AR6 projections for regional climate change in the Middle East region. The temperature increments used for future projections for the year 2050 are: SSP2-4.5 (moderate emissions) SSP5-8.5 (high emissions).

4 RESULTS AND DISCUSSION

4.1 Land Use / Land Cover Maps

The Land Use/Land Cover (LU/LC) maps for the years 2009, 2014, 2019, and 2024 were produced using the Maximum Likelihood Method to ensure good performance in the classification of the land. The accuracy assessment of the Land Use/Land Cover maps was done. In this regard, the produced maps were validated using the maximum likelihood method, with accuracy being determined using the kappa coefficient and overall accuracy. From the results, it is clear that all the maps have high accuracy, as they are within the acceptable range. The kappa indices for the years 2009, 2014,2019 and 2024 are given as 89%, 85.8%, 84.7%, and 87.1%, respectively. (Table 3)

YEARS	2009	2014	2019	2024
Overall Accuracy %	94.7	92.7	92.5	91.4
Kappa Index %	89	85.8	84.7	87.1

Table 3: Accuracy assessment of land use/cover for 2009, 2014, 2019, and 2024.

LU/LC maps for 2009, 2014, 2019, and 2024 were produced to reveal the spatial and temporal dynamics of land transformation in Erbil city. From the results (Figure 3), it is clear that there has been an increase in built-up land, with a corresponding decrease in barren land. This shows that there has been rapid growth over the years.

In 2009, barren land was dominant, with 513.14 km² (79.40%) of the total area, followed by built-up land, which was 125.49 km² (19.42%), and then vegetation land, which was 7.61 km² (1.18%). By 2014, built-up land was 174.06 km² (26.93%), barren land was 456.78 km² (70.68%), and vegetation land was 15.40 km² (2.38%). This trend continued in 2019, with built-up land increasing to 186.65 km² (28.88%), barren land decreasing to 434.70 km² (67.26%), and vegetation land increasing to 24.90 km² (3.85%). By 2024, built-up land continued to increase, reaching 187.69 km² (29.04%), vegetation land reached 26.16 km² (4.05%), and barren land continued to decrease, reaching 432.40 km² (66.91%) (Table 4) (Figure 3).

Over the period from 2009 to 2024, the built-up land increased by 62.19 km², from 19.42% to 29.04%. The bare land decreased by 80.75 km², from 79.40% to 66.91%. The vegetation land increased by 18.55 km², from 1.18% to 4.05%. These changes demonstrate the high influence of the urban expansion and land conversion processes. so (Weng, 2009; El-Zeiny and Effat, 2017; Rasul, Balzter and Smith, 2017). which are well established in literature and in the study using the Landsat satellite imagery. The results are also in agreement with the urban growth observed in the study area and in other semi-arid regions.

The factors that influenced the increase in the urban land use are the declaration of Erbil as the capital of the Kurdistan Region on the 20th of March, with political and economic factors being the major factors influencing the growth in the study area.(Ibrahim, R.I., Mushatat, S.A. and Abdelmonem, M.G. 2015)

class name	Area km² 2009	area %	Area km² 2014	area %	Area km² 2019	area %	Area km² 2024	area
Barren land	513.14	79.40	456.78	70.68	434.70	67.26	432.40	66.91
vegetation land	7.61	1.18	15.40	2.38	24.90	3.85	26.16	4.05
build - up land	125.49	19.42	174.06	26.93	186.65	28.88	187.69	29.04
total	646.25	100.00	646.25	100.00	646.25	100.00	646.25	100.00

Table 4: Quantity of land use and land cover.

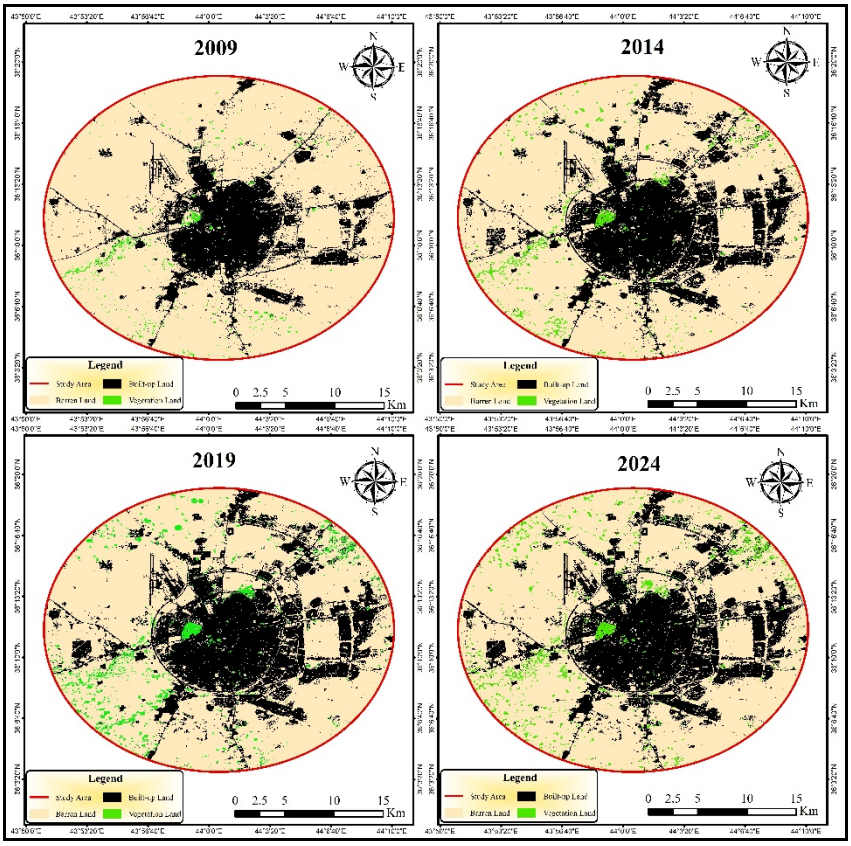

Figure 3: Supervised classification of land use and land cover

4.2 Land Surface Temperature (LST) Distribution (2009-2024)

Figure 4 shows the distribution of Land Surface Temperature (LST) in Erbil for 2009, 2014, 2019, and 2024. The maps show the progressive increase of temperature hotspots in the study area. The hottest temperature zones in each map were consistently concentrated in the bare or sparsely vegetated surfaces of the study area, while the coldest temperature zones were consistently concentrated in the vegetated zones of the study area.

In 2009, the temperature range was between 32°C and 51°C. The hottest temperature zones were consistently concentrated in the bare or sparsely vegetated surfaces of the study area, particularly in the western to northwestern zones of the study area. The coldest temperature zones were consistently concentrated in the vegetated zones of the study area, particularly around the urban area. In 2014, the temperature range was between 33.9°C and 52°C. In 2019, the temperature range was between 33.5°C and 52.6°C. In 2024, the temperature range was between 34.6°C and 54.3°C. The hottest temperature zones were consistently concentrated in the bare or sparsely vegetated surfaces of the study area, particularly in the western, southwestern, and northeastern zones of the study area. The coldest temperature zones were consistently concentrated in the vegetated zones of the study area. Sami Abdul Rahman Park was consistently one of the coldest temperature zones in 2009 and 2024.

The relatively lower temperature zones identified in the city center during the morning satellite overpass time (07:00-09:00) can be related to Surface Urban Cool Island (SUCI) phenomenon identified in other urban areas in the world, especially in the context of the study in the city of Erbil. The dry season in the rural/barren surfaces surrounding the study area shows efficient surface heating because of low moisture content and scarce shading. In contrast, relatively lower temperature zones can be present in urban surfaces during the daytime and morning periods, especially in urban surfaces with higher surface wetness and vegetation(Rasul, Balzter and Smith, 2015; Rasul, Balzter and Smith, 2016). The high amount of cement and concrete used in the surfaces in Erbil also affects the surface temperature response in the early morning. The high thermal mass of concrete allows for the storage of heat, which moderates extreme changes in temperature. (Concrete Society, 2025) Therefore, after the nocturnal cooling period, these surfaces can remain relatively cooler in the early morning compared to dry bare surfaces.

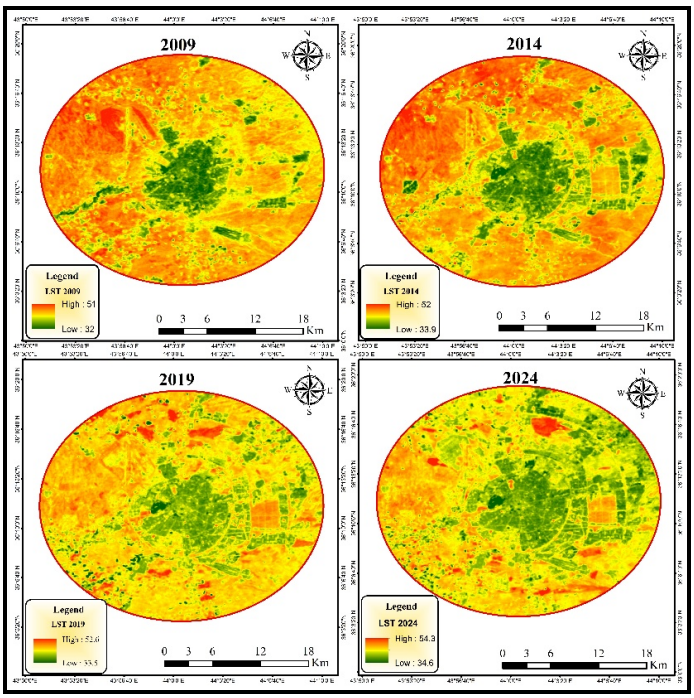

Figure 4: land surface temperature map extract in thermal band of Landsat

4.3 NDVI Spatial Pattern (2009-2024)

The spatial distribution of Normalized Difference Vegetation Index (NDVI) for the city of Erbil in 2009, 2014, 2019, and 2024 is depicted in Figure 5. The figure reveals the differences between vegetated surfaces and non-vegetated surfaces. In 2009, NDVI values varied between -0.37 and 0.73. The higher NDVI values were limited to small patches of green. The majority of the area was characterized by low NDVI values, i.e., near zero. In 2014, NDVI values varied between -0.32 and 0.78. The patches of green were more noticeable in the urban area. The situation remained more or less the same in 2019, with NDVI values ranging between -0.27 and 0.80. In 2024, NDVI reached its maximum value of 0.84. The NDVI values reached their lowest in 2024, i.e., -0.22. The spatial distribution of NDVI in the urban area of Erbil in all four years reveals that the maximum NDVI values are concentrated in Sami Abdulrahman Park.

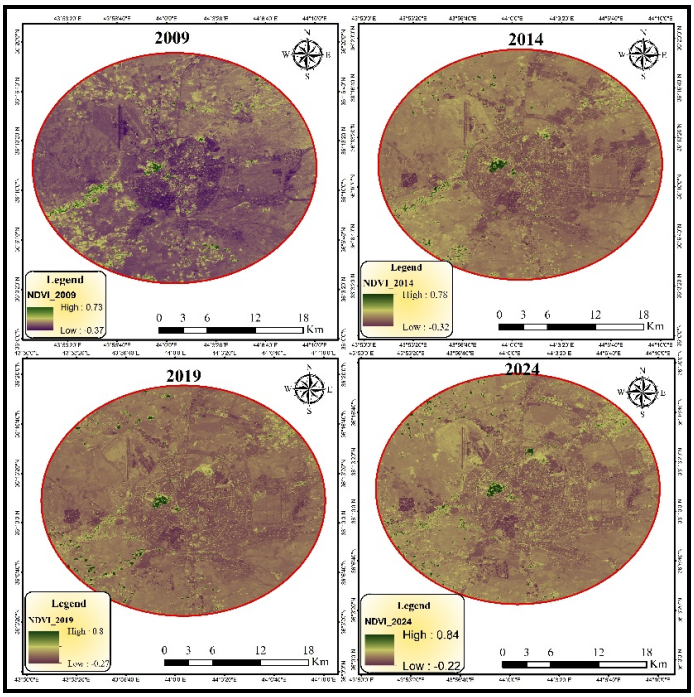

Figure 5: Normalized Difference Vegetation Index In 2009,2014,2019 And 2024.

4.4 Urban Heat Island (UHI) Intensity (2009-2024)

Figure 6 illustrates the spatial distribution of the Surface Urban Heat Island (UHI) intensity for the years 2009, 2014, 2019, and 2024. As depicted, the Urban Heat Island intensity has increased significantly.

In 2009, the Urban Heat Island intensity varies from -11.3°C to 14.6°C, and the maximum value of the Urban Heat Island occurs in the central region of the study area. This value increases to 18.4°C in 2014 and to 22.5°C in 2019. In 2024, the value of the Urban Heat Island has reduced to 19.4°C. Strong hotspots appear in the central built-up areas and the expanding areas of the west and southwest, while the minimum and negative values appear in the vegetated areas, such as Sami Abdul Rahman Park, and the rural areas to the north and west of the study area.

It is clear that the difference between the hottest areas and the coolest areas of the study area is approximately 28% of the surface thermal range.(Chakraborty, T. and Lee, X. 2019).

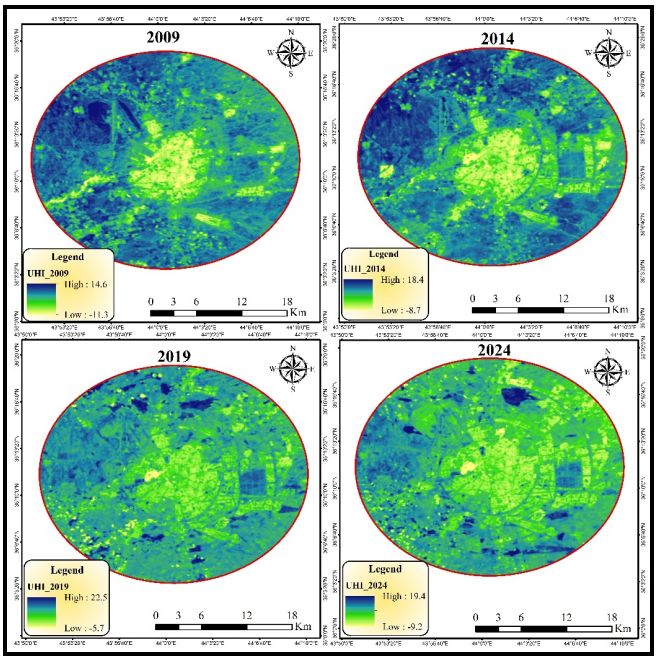

Figure 6: Spatial distribution of Surface Urban Heat Island (UHI) intensity in Erbil city for 2009, 2014, 2019, and 2024.

4.5 Observed and Projected Changes in Land Surface Temperature in Erbil under SSP2-4.5 and SSP5-8.5

According to Table 5 and the above-mentioned line chart (Figure 7), there is an obvious upward trend observed in the land surface temperature (LST) of Erbil from 2009 to 2050 under the above-mentioned climate change scenarios. It is observed that the range of temperature in Erbil was between 32°C (minimum) and 51°C (maximum) in 2009. However, this range of temperature has increased over the years, reaching 34.6°C (minimum) and 54.3°C (maximum) by 2024. This shows an upward trend over the last 15 years. This trend is expected to increase over time. Under the intermediate scenario of SSP2-4.5, the LST of Erbil is expected to rise to 35.0°C (minimum) and 55.0°C (maximum) by 2050. Under the high scenario of SSP5-8.5, the LST of Erbil is expected to rise to 35.4°C (minimum) and 56.7°C (maximum) by 2050. This shows an increase in the minimum and maximum temperature of Erbil, with the maximum temperature rising more under the high scenario of SSP5-8.5. It is worth mentioning here that this projection has been done under a business-as-usual scenario, i.e., no green belt has been considered.

year	Minimum LST (°C)	Maximum LST (°C)
2009	32	51
2014	33.9	52
2019	33.5	52.6
2024	34.6	54.3
2050 SSP4.5	35	55.046
2050 SSP8.5	35.4	56.7

Table 5 : Minimum and Maximum Land Surface Temperature (°C) for Historical Years and 2050 Climate Scenarios

Editors: M. Schrenk, C. Beyer, T. Popovich, J. Ryser, D. Mawlood
ISBN 978-3-9504945-5-6

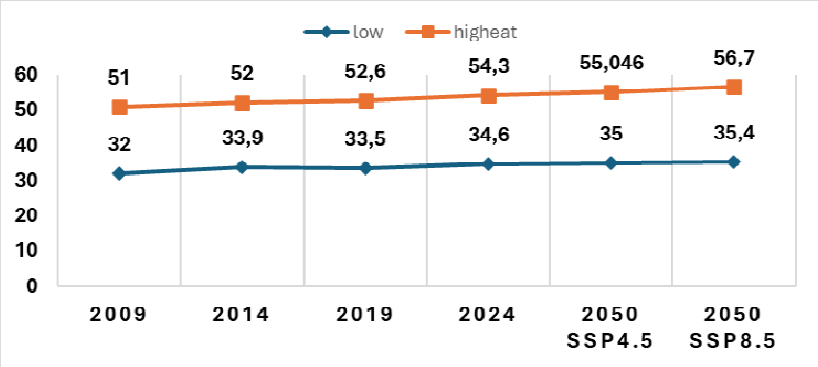

Figure 7: Minimum and Maximum Land Surface Temperature (°C) for Historical Years and 2050 Climate Scenarios

4.6 Green Belt Master Plan Scenario (2050)

In order to mitigate the expected increase in Land Surface Temperature (LST) under SSP2-4.5 and SSP5-8.5 scenarios, a Green Belt master plan was developed around the Erbil city area. The Green Belt area is approximately 165.35 km² in size, with 7.2 million olive and pistachio trees being planted. The tree density is approximately 435 trees per hectare with an inter-tree distance of about 4.8 meters. The present Normalized Difference Vegetation Index (NDVI) is 0.17 in the Green Belt area, which indicates a very sparse vegetation cover with a semi-arid surface.

Based on studies of orchard vegetation, NDVI ranges between 0.25 and 0.45 for young or low-irrigation orchards of olive/pistachio varieties. NDVI ranges between 0.45 and 0.65 for mature orchards with good irrigation conditions. NDVI > 0.75, which indicates very dense forest conditions, is not realistic in a semi-arid orchard. (Pettorelli et al., 2005; Barajas et al., 2020). Therefore, a very moderate NDVI of 0.5 was selected for the Green Belt scenario in 2050.

Using the established NDVI-LST regression model (LST = 54.60 - 5.01*NDVI), the NDVI was increased to 0.5. The expected direct cooling effect in the Green Belt area is estimated at -2.5 °C. The indirect cooling effect in the urban area is estimated at -0.4 °C. The NDVI-enhanced LST distribution under the Green Belt scenario is presented in Figure 8.

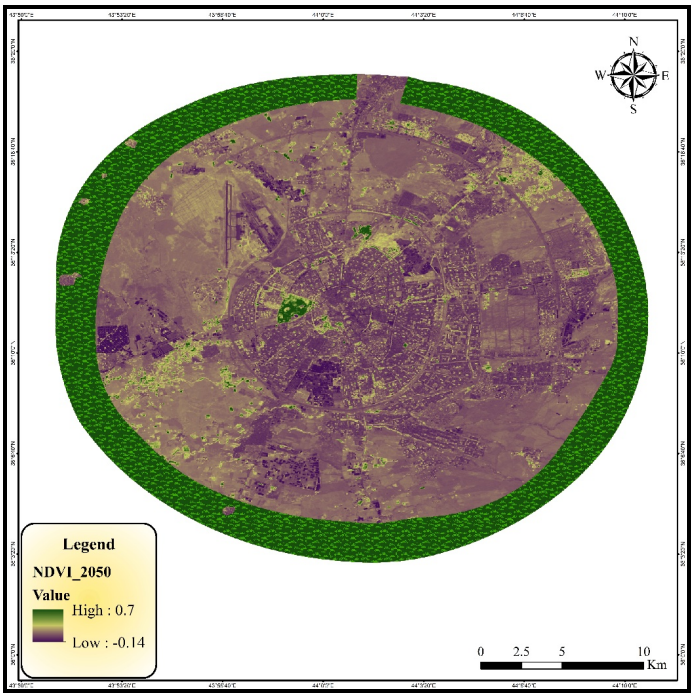

Figure 8: Simulated NDVI Distribution under the 2050 Green Belt Master Plan Scenario (Erbil City)

5 CONCLUSION

Quantification of the interaction between urban growth, vegetation, and surface temperature was done, and future land surface temperature under conditions of climate change was also modeled. The results showed

that rapid growth has significantly changed the surface energy balance of Erbil. The results also showed that the increase of built-up area was 62.19 km², with most of the change being from barren land. Vegetation change was very low. This has, therefore, increased the maximum temperature from 51°C in 2009 to 54.3°C in 2024, with an increase of the urban heat island effect, especially in the western and southwestern parts of the city.

From the scenario modeling, it was also observed that the maximum temperature would increase by 2050. This increase would be to 55.0°C under SSP2-4.5 and 56.7°C under SSP5-8.5.

From the Green Belt master plan scenario, it was observed that there was an opportunity for mitigation. This was done by elevating the normalized difference vegetation index (NDVI) from 0.17 to 0.5 through large-scale plantation of olive and pistachio trees. This would result in a decrease of 2.5°C within the Green Belt and 0.4°C at the city scale. This shows that there is an opportunity for mitigating future temperature rise through strategic planning.

From the results, therefore, it was observed that there was a need to develop a framework for addressing future temperature rise. This can be done through strategic planning, which would also be very useful for enhancing the resilience of the city of Erbil and other semi-arid cities.

6 REFERENCES

BARAJAS, E.; ÁLVAREZ, S.; FERNÁNDEZ, E.; VÉLEZ, S.; RUBIO, J.A.; MARTÍN, H.: Sentinel-2 satellite imagery for agronomic and quality variability assessment of pistachio (Pistacia vera L.). In: Sustainability, Vol. 12, Issue 20, 8437. 2020.

BELGIU, M.; DRĂGUŢ, L.: Random forest in remote sensing: A review of applications and future directions. In: ISPRS Journal of Photogrammetry and Remote Sensing, Vol. 114, pp. 24–31. 2016.

BREIMAN, L.: Random forests. In: Machine Learning, Vol. 45, Issue 1, pp. 5–32. 2001.

CHAKRABORTY, T.; LEE, X.: A global database of surface urban heat island intensity. In: Scientific Data, Vol. 6, 280. 2019.

CONGALTON, R.G.; GREEN, K.: Assessing the Accuracy of Remotely Sensed Data: Principles and Practices. 3rd edn. Boca Raton, FL, 2019.

EL-ZEINY, A.M.; EFFAT, H.A.: Environmental monitoring of spatiotemporal change in land use/land cover and its impact on land surface temperature. In: Remote Sensing Applications: Society and Environment, Vol. 8, pp. 266–277. 2017.

HERSBACH, H. et al.: The ERA5 global reanalysis. In: Quarterly Journal of the Royal Meteorological Society, Vol. 146, Issue 730, pp. 1999–2049. 2020.

HUSSEIN, S.O.; KOVÁCS, F.; TOBAK, Z.: Spatiotemporal Assessment of Vegetation Indices and Land Cover for Erbil City and Its Surrounding Using Modis Imageries. In: Journal of Environmental Geography, Vol. 10, Issue 1–2, pp. 31–39. 2017.

IBRAHIM, R.I.; MUSHATAT, S.A.; ABDELMONEM, M.G.: Erbil. In: Cities, Vol. 49, pp. 14–25. 2015.

IPCC: Climate Change 2021: The Physical Science Basis. Contribution of Working Group I to the Sixth Assessment Report of the Intergovernmental Panel on Climate Change. Cambridge, 2021.

ITURBIDE, M. et al.: An update of IPCC climate reference regions for subcontinental analysis of climate model data. In: Earth System Science Data, Vol. 13, pp. 2959–2970. 2021.

JENSEN, J.R.: Introductory Digital Image Processing: A Remote Sensing Perspective. 4th edn. Pearson, 2015.

JULIEN, Y.; SOBRINO, J.A.: The Yearly Land Cover Dynamics (YLCD) method: An analysis of global vegetation from NDVI and LST parameters. In: Remote Sensing of Environment, Vol. 113, Issue 2, pp. 329–334. 2009.

KARNIELI, A. et al.: Use of NDVI and land surface temperature for drought assessment: Merits and limitations. In: Journal of Climate, Vol. 23, Issue 3, pp. 618–633. 2010.

KOVÁCS, F.; TOBAK, Z.: Urban growth and environmental risks in Erbil City. In: International Conference on Climate Change and Their Environmental Risks from Geographical Perspective. 2017.

LI, X.; ZHOU, Y.; ASRAR, G.R.: Response of surface urban heat island to urban expansion: A remote sensing perspective. In: Remote Sensing, Vol. 12, Issue 5, 812. 2020.

LI, X.; ZHOU, Y.; ASRAR, G.R.; IMHOFF, M.; LI, X.: The surface urban heat island response to urban expansion: A panel analysis for the conterminous United States. In: Science of the Total Environment, Vol. 605–606, pp. 426–435. 2019.

MUÑOZ-SABATER, J. et al.: ERA5-Land: A state-of-the-art global reanalysis dataset for land applications. In: Earth System Science Data, Vol. 13, pp. 4349–4383. 2021.

OKE, T.R.: The energetic basis of the urban heat island. In: Quarterly Journal of the Royal Meteorological Society, Vol. 108, Issue 455, pp. 1–24. 1982.

PETTORELLI, N.; VIK, J.O.; MYSTERUD, A.; GAILLARD, J.M.; TUCKER, C.J.; STENSETH, N.C.: Using the satellite-derived NDVI to assess ecological responses to environmental change. In: Trends in Ecology & Evolution, Vol. 20, Issue 9, pp. 503–510. 2005.

QIN, Z.; KARNIELI, A.; BERLINER, P.: A mono-window algorithm for retrieving land surface temperature from Landsat TM data and its application to the Israel-Egypt border region. In: International Journal of Remote Sensing, Vol. 22, Issue 18, pp. 3719–3746. 2001.

RASUL, A.; BALZTER, H.; SMITH, C.: Applying a normalized ratio scale technique to assess influences of urban expansion on land surface temperature of the semi-arid city of Erbil. In: International Journal of Remote Sensing, Vol. 38, Issue 13, pp. 3960–3980. 2017.

RASUL, A.; BALZTER, H.; SMITH, C.: Diurnal and seasonal variation of surface urban cool and heat islands in the semi-arid city of Erbil, Iraq. In: Climate, Vol. 4, Issue 3, 42. 2016.

RICHARDS, J.A.; JIA, X.: Remote Sensing Digital Image Analysis: An Introduction. 4th edn. Berlin, 2006.

RONGALI, G.; KESHARI, A.K.; GOSAIN, A.K.: Evaluation of land surface temperature retrieval methods and NDVI–LST relationship. In: Journal of Earth System Science, Vol. 127, Issue 2, pp. 1–16. 2018.
SANTAMOURIS, M.: Analyzing the heat island magnitude and characteristics in one hundred Asian and Australian cities and regions. In: Renewable and Sustainable Energy Reviews, Vol. 38, pp. 47–63. 2015.
SETO, K.C.; GÜNERALP, B.; HUTYRA, L.R.: Global forecasts of urban expansion to 2030 and direct impacts on biodiversity and carbon pools. In: Proceedings of the National Academy of Sciences, Vol. 109, Issue 40, pp. 16083–16088. 2012.
SOBRINO, J.A.; JIMÉNEZ-MUÑOZ, J.C.; PAOLINI, L.: Land surface temperature retrieval from Landsat TM 5. In: Remote Sensing of Environment, Vol. 90, Issue 4, pp. 434–440. 2004.
U.S. GEOLOGICAL SURVEY (USGS): Landsat (OLI/TIRS) mission and sensor information. Available at: https://www.usgs.gov/landsat-missions/landsat-9.
UNITED NATIONS, DEPARTMENT OF ECONOMIC AND SOCIAL AFFAIRS, POPULATION DIVISION: World Urbanization Prospects: The 2018 Revision. New York, 2019.
VOOGT, J.A.; OKE, T.R.: Thermal remote sensing of urban climates. In: Remote Sensing of Environment, Vol. 86, Issue 3, pp. 370–384. 2003.
WENG, Q.: Thermal infrared remote sensing for urban climate and environmental studies: Methods, applications, and trends. In: ISPRS Journal of Photogrammetry and Remote Sensing, Vol. 64, Issue 4, pp. 335–344. 2009.
WENG, Q.; LU, D.; SCHUBRING, J.: Estimation of land surface temperature–vegetation abundance relationship for urban heat island studies. In: Remote Sensing of Environment, Vol. 89, Issue 4, pp. 467–483. 2004.
YUE, W. et al.: The relationship between land surface temperature and NDVI with remote sensing: Application to Shanghai Landsat 7 ETM+ data. In: International Journal of Remote Sensing, Vol. 28, Issue 15, pp. 3205–3226. 2007.
ZHANG, H.; QI, Z.F.; YE, X.Y.; CAI, Y.B.; MA, W.C.; CHEN, M.N.: Analysis of land surface temperature based on random forest regression. In: Remote Sensing, Vol. 9, Issue 4, 349. 2017.
ZHOU, D.; ZHAO, S.; LIU, S.; ZHANG, L.; ZHU, C.: Surface urban heat island in China's 32 major cities: Spatial patterns and drivers. In: Remote Sensing of Environment, Vol. 152, pp. 51–61. 2014.